This is a repository copy of *Experimental investigation of transient ignition dynamics of hydrogen enriched methane diffusion impinging flames*.

White Rose Research Online URL for this paper:
https://eprints.whiterose.ac.uk/171757/

Version: Accepted Version

Article:

Experimental Investigation of Transient Ignition Dynamics of Hydrogen Enriched Methane Diffusion Impinging Flames

Q. Wang[a] (✉), X.H. Mei[a], Z.Y. Wei[b], C.Y. Zhao[a], Y. Zhang[c]

[a] *School of Mechanical Engineering, Shanghai Jiao Tong University, Shanghai, 200240, China*

[b] *China-UK Low Carbon College,* Shanghai Jiao Tong University, Shanghai, 200120, China

[c] *Department of Mechanical Engineering, University of Sheffield, Mappin Street, Sheffield, S1 3JD, UK*

Corresponding author: qianwang@sjtu.edu.cn

Phone: +86(21)34204541

Fax: +86(21)34206092

Abstract

The ignition characteristics of hydrogen enriched methane diffusion impinging flames are investigated experimentally. Keeping the total fuel flow rate constant, the hydrogen volume percentage is set at 40% and 60% respectively, while a pure methane flame is also involved for comparison. Two traditional optical diagnostics, high speed colour and schlieren imaging techniques have been used to tackle the fast transient ignition process with advanced digital image processing algorithms. The weak blue flame during the ignition process, which is hardly seen on the original high speed images, has been enhanced selectively to reveal the complete flame structure. The flow field velocity during the ignition process has been estimated using an optimised schlieren motion estimation method. The relative velocity between the flame and flow velocities has also been resolved and analysed. The results indicate that the flow field velocity increases with increasing hydrogen percentage. The maximum velocity detected in the test cases can be as high as over 3.5 m/s when the hydrogen volume percentage is at 60%. The techniques used in the current study are simple to set up and convenient to use, which have shown

enormous potential to be applied in the experimental investigations into more complex combustion configurations.

Keywords: Ignition; Impinging flame; High speed imaging ; Schlieren velocimetry.

1. Introduction

High efficiency combustion with clean fuels has been investigated intensively, due to the concern of increasing energy demand and pollutant emission reduction. Natural gas is a promising candidate for engines, power plants and other industrial applications [1]. The major component of natural gas is methane, while the compositions may vary in the fuel from different sources. The molecular structure of methane is tetrahedral and the C-H bond energies are relatively high, which has induced some unfavourable characteristics for the ignition process, including high ignition temperature and low flame propagation speed [2]. On the counterpart, hydrogen owns the advantages of low ignition energy, high reactivity, high diffusivity and fast burning velocity. Thus it is an effective solution to improve the ignition characteristics by adding a certain percentage of hydrogen into methane. The combustion characteristics of premixed methane-hydrogen-air flames has been measured and analysed with various hydrogen fractions [3, 4]. It is found that the laminar burning velocity increases with the hydrogen percentage in a linear trend, while the H, O and OH radical mole fractions are found to increase accordingly.

The ignition process is a fundamental research topic in combustion science, which addresses the transition from a non-reacting to a fully burning state and may affect the combustion efficiency and exhaust emissions of practical combustion devices, such as aeroengines, spark-ignition engines and diesel engines. The initiation of turbulent non-premixed flames through autoignition and spark ignition has been reviewed by Mastorakos [5]. Phuoc et al. [6] pointed out that for the spark initiated combustion, the success of ignition is determined by whether the reacting gas could transit from hot plasma to a propagating flame or not. The simulation work by Richardson and Mastorakos [7] indicates that the ignition can be prohibited by excessive strain rates in a non-premixed flame. The direct

2

numerical simulation study conducted by Jin et al. [8] in a turbulent dimethyl ether (DME)/methane-air mixture mixing layer indicated that the formation and propagation of multiple triple flames along the stoichiometric mixture has essential effects on the flame developing process. Also adding DME helps to reduce the time required for the initiation of steady flame due to its higher reactivity than methane. Rajpara et al. [9] conducted both experimental and large eddy simulation (LES) studies of hydrogen enriched methane flames in an upward swirl can combustor under both constant heat input and constant volumetric flow rate conditions. The results have shown that the velocity, temperature and NO_x emissions are increased when the hydrogen percentage is increased but the total heat input is the same. When the total volumetric flow rate is kept constant, the hydrogen enriched flames would become narrower and shorter, while the NO_x emissions were slightly increased. Hussain et. al. [10] investigated the secondary injection of hydrogen to imperfectly premixed methane and ethylene flames in a bluff-body combustor under acoustic perturbations. It is found that adding hydrogen can help to reduce the heat release oscillations and thus combustion instability. Recently, Oztarlik et al. [11] investigated the impact of hydrogen addition strategy on the dynamics of a premixed methane flame in a swirled injector. The results indicated that when using pure hydrogen as the pilot fuel, with only a small amount, the unstable zones can be significantly reduced. However, if the same amount of hydrogen is fully premixed with methane and air, there is no change in the stability map.

Flame impingement on solid walls are widely used in many industrial occasions, including metal processing, glass making, welding, and so on. It also exists in confined combustion chambers, which may affect the combustion characteristics, heat transfer and emissions. Due to the complex flame-to-wall interactions, the ignition characteristics of impinging flames have very different features from those of the widely investigated free jet flames [12]. The flame establishment under impinging conditions can be affected by multi factors, including jet flow condition, nozzle to wall distance, ignition initiation position as well as fuel compositions [13-16]. Wang et al. investigated the ignition process of a diffusion propane and a methane impinging flame using high speed colour and schlieren imaging techniques [17, 18], respectively. Chen et al. [19] conducted a numerical study using LES on

the ignition process of diffusion impinging propane flames, which reached qualitative agreement with the experimental observations reported by Wang et al. [18]. Moreover, their results indicated that although a non-premixed jet flame is specified at the inlet, both premixed and non-premixed combustion modes exist in the turbulent impinging flames during the ignition process and in the near-wall region. When ignited at different locations, the flow and mixing processes are strongly affected by the thermal expansion triggered by ignition in premixed flame regions, which in turn leads to different flame dynamics subsequently. It is seen that previous studies on the ignition process of impinging flames were mainly concentrated on single-component fuels. However, variations in fuel composition would have significant effects on the ignition characteristics. To the best of the authors' knowledge, the ignition process of methane and hydrogen mixtures with different compositions under impinging flame conditions has not been reported so far, which merits systematic investigations to enhance our understanding of the complex ignition process.

Ignition is a transient process which occurs in a very short time, normally in dozens or hundreds of milliseconds. Visualization of the rapid changing flame and flow field structure is essential to understand the complex phenomena, which requires high frame rate optical diagnostics. Although nowadays kHz laser diagnostics is capable of supplying quantitative data, full-field imaging of ignition and the subsequent flame development is still hard to achieve. In addition, such laser diagnostics is inherently complex to set up and expensive to run. In the current study, we use two synchronised high speed cameras to capture the colour and schlieren images simultaneously. Besides flow visualisation from the images, advanced image processing techniques are applied to retrieve quantitative information, which is essential for deeply understanding the transient ignition process. The digital colour images encode the incident radiation into three discrete bands of signal wavelengths peaking in the R, G and B (red, green and blue) portions of the visible electromagnetic spectrum, which simulates the human visual system. Thus, the digital colour imaging technique for flames can be considered as a multi-spectral device, which offers simultaneous two dimensional information in the captured images. With the aid of a high speed camera, the technique also features excellent resolution in time domain.

However, during the past decades, the colour images are mostly used for only qualitative visualisation. The rich spectral information hidden in the digital signals was not adequately explored. For hydrocarbon flames, there are mainly two types of flames that can be discriminated from the visible spectra regime offered by colour images [20]. One type is the blue-green flame, which mainly exists in the premixed flame region, showing good consistency with the CH* and C_2* chemiluminescence intensities. The other type is the yellow-reddish colour from the solid carbon/soot emission, which represents the non-premixed flame region. Huang et al. [21] have established a Digital Flame Colour Discrimination (DFCD) combustion quantification scheme to identify different flame regimes based on the general spectrometric composition. The previous study [17, 18] indicated that during the initial stage of the ignition process of hydrocarbon flames, there is large amount of weak blue flame, which can hardly be observed with the original high speed colour image. However, the flame structure can be fully revealed using the DFCD method.

Schlieren is another commonly used optical technique for flow visualization, which records the flow pattern due to the refractive index change when passing through the inhomogeneous test flow field [20]. It requires only a common light source, has very short shutter speed (μs) and enables the maximum frame rate of a high speed camera. It features low cost, good sensitivity and no requirement for seeding particles. Over the past decades, considerable efforts have been made to develop quantitative velocimetry algorithms based on high speed schlieren sequences [23-25]. Recently, Wang et al. [26] have proposed a schlieren motion estimation (SME) method, which supplies a dense estimate of the motion at each pixel. The results indicate that, compared with other optical flow methods, SME is able to resolve more details in the flow field; the results show better continuity in the main flow region and also the shear layers.

In this paper, the ignition process of methane/hydrogen diffusion flames is investigated experimentally under impinging conditions, using the aforementioned techniques. The novelty of the present study mainly lies in two aspects. Firstly, the hydrogen percentage effect on the fast transient

ignition process of impinging flame is revealed by the experimental results. The effects of fuel composition variation on flow pattern, flow speed, flame propagation as well as soot formation are analysed comprehensively, which is valuable to fundamental research on spark ignition and can also be served as useful validation data for numerical modeling studies. Secondly, the techniques employed are adaptable to industrial test environment, which can be applied in practical systems to investigate the hydrogen enriched combustor emissions and stabilities.

2. Experimental methods

2.1 Experimental setup

The schematic layout of the experimental apparatus is shown in Fig. 1. The impinging flame configuration consists of a burner and a solid plate. The fuel is supplied from the central nozzle of the burner. The nozzle is round in shape and has an inner diameter (d_n) of 8 mm. The solid plate disc is made of steel, with 300 mm in diameter and 10 mm in thickness. The plate is kept at a distance of 150 mm from the nozzle exit, which corresponds to a normalized distance with respect to the fuel nozzle diameter of 18.75 d_n. In the experiments, methane and hydrogen mixtures were fed into the burner nozzle, while their flow rates were dedicatedly controlled by flow controllers using the Labview 10.0 software. In this study, the fuel flow rate is fixed at 10 l/min, which induces an exit velocity of 3.32 m/s. The composition of the fuel mixture varies from pure methane to rich hydrogen percentages, which has been listed in Table 1. Due to the composition variances, the Reynolds number is changing in a range from 590 to 1567. The Reynolds number is decreasing with higher hydrogen volume percentage mainly due to its much smaller density.
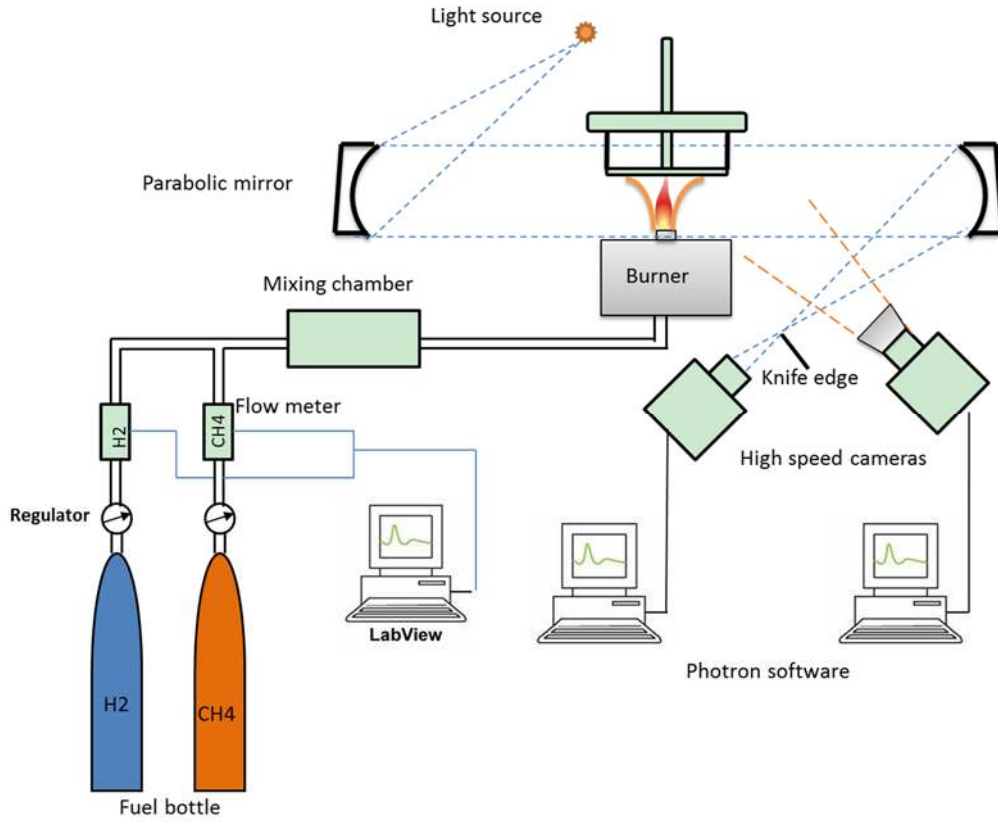
Fig. 1 Schematic of experiment setup

Table 1 Test conditions

Case	Volume Percentage		Density (ρ)	Viscosity ($\mu \cdot 10^6$)	Re
	CH$_4$	H$_2$	(kg/m^3)	(N$\cdot$s/m^2)	
Methane	/	/	0.659	11.17	/
Hydrogen	/	/	0.0827	8.35	/
m10h0	100%	0%	0.659	11.17	1567
m6h4	60%	40%	0.428	10.04	1133
m4h6	40%	60%	0.313	9.48	878

For the acquisition of schlieren images, a z-type schlieren mirror arrangement has been utilized, which consists of a 500 W Xenon lamp source, two parabolic mirrors and a vertical knife edge. The parabolic mirrors have a diameter of 0.3048 m (12 in.) and a focal length of 3.048 m (10 feet). Two high speed cameras were synchronised using the master-slave mode, which can restrict the time delay less than 0.5 μs. The schlieren images were captured by a high-speed monochromic imaging camera (Photron Fastcam XLR-1024), from a direction perpendicular to the plate. The shutter speed for schlieren imaging is set at 1/100,000 s and the frame rate is 1000 fps. The other high speed digital colour camera (Photron SA4) was utilized to capture the flame establishment process from the instance of ignition. In order to observe more flame structures, the camera is positioned with a tilted view angle, as shown in Fig.1. The colour camera was set at 250 fps for frame rate and 1/250 s for shutter speed. Both the colour and schlieren images were taken at the maximum resolution of 1024 by 1024 pixels.

An electric spark igniter is remade from a motorcycle spark plug, while the plug is replaced by two needle electrodes. A sealed lead acid battery (12 volt, 1.2 Ah) is utilized as the power source, which supplies electric charge to the high voltage coil. A high voltage (~30 kV) is generated consistently and applied on the two electrodes, which were located tip to tip with a gap of 6 mm. The igniter of this type can supply a pulsed spark with the energy around 10 mJ. The distance from the nozzle exit to the igniter is 7 mm.

2.2 Image processing of the colour images

Previous colour analysis on the hydrocarbon flame images indicates that it is able to identify and separate the bluish and yellowish flame regions by setting filters using hue value within the HSV (Hue, Saturation and Value) colour model space [21]. Thus the first step is to resolve the hue value (H) of the recorded colour images by transferring the images from RGB model into HSV model following the equations below:

$$H^{''} = \begin{cases} \dfrac{G-B}{Max-Min} & if \quad R = Max \\ 2 + \dfrac{B-R}{Max-Min} & if \quad G = Max \\ 4 + \dfrac{R-G}{Max-Min} & if \quad B = Max \end{cases} \tag{1}$$

$$H^{'} = \frac{H^{''}}{6} \times 360 \tag{2}$$

$$H = \begin{cases} H^{'} & if \quad H^{'} > 0 \\ H^{'} + 360 & if \quad H^{'} < 0 \end{cases} \tag{3}$$

The colour analysis with different types of methane flames revealed that the premixed flame can be well filtered out using the hue value (H) ranging from 180° to 300°. After the identification, the blue flame will be selected and enhanced, by amplifying the R, G, B intensities 15 times of the original values respectively. An original and the corresponding blue colour-enhanced image has been shown in Fig. 2 for comparison. The images show the flame structure of m6h4 at 60 ms after ignition. The processed image has shown that the bluish flame has a comparable area with the yellowish flame; but it can hardly be seen on the original image. The interpretation of high speed or high shutter speed flame colour images directly may be quite misleading, especially when some part of the flame is much weaker than the other parts.
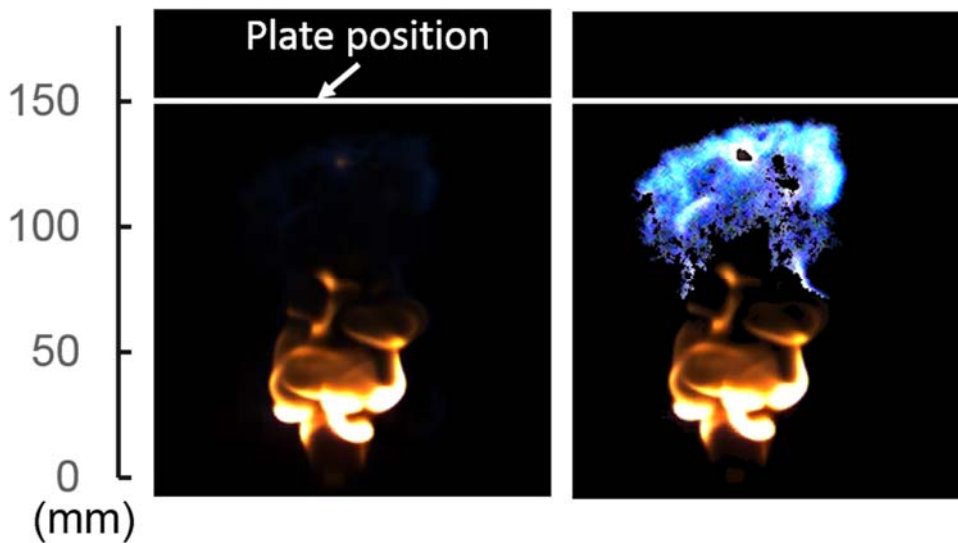

Fig. 2 Comparison between the original (Left) and the blue colour-enhanced images (Right)
(m6h4 at 60 ms after ignition)

2.3 Turbulent flow field velocimetry using schlieren images

The velocity fields during the ignition process have been extracted from the schlieren estimation method (SME), which is proposed as an optimized optical flow technique. In order to resolve the two dimensional velocity components u and v, two basic constraints are required to establish the equations: one is the constancy constraint and the other is the smoothness constraint. In SME method, a physical-oriented constancy constraint is adopted by combining the schlieren luminance characteristics and the continuity equations, which is

$$\frac{dI}{dt} + \frac{I}{2}\left(\frac{\partial v}{\partial x} + \frac{\partial u}{\partial y}\right) = 0 \,, \tag{4}$$

where I is the image intensity, t is the time between frames, u and v are velocity components in x and y directions. The detailed derivation and justification of Eq.(4) can be found in [26]. A second order div-curl constraint proposed by Suter et al. [24] is used as the smoothness constraint, which enables the preservation of more fluid structures:

$$R = \left|\nabla\text{div}\vec{V}\right|^2 + \left|\nabla\text{curl}\vec{V}\right|^2 \tag{5}$$

where $\text{div}\vec{V} = \frac{\partial u}{\partial x} + \frac{\partial v}{\partial y}$ and $\text{curl}\vec{V} = \frac{\partial v}{\partial x} - \frac{\partial u}{\partial y}$ are the divergence and vorticity of velocity field, respectively. To deal with the computational difficulties of second order smoothness functional implementation, the approach proposed in [28, 29] is followed. This leads to a regularization term in two interleaved first-order div-curl regularizations based on two auxiliary scalars to approximate the divergence and the vorticity of the flow.

Based on the two constraints listed by Eqs. 4 and 5, the global cost funcion is established and optimized using a variation method. Several advanced optimization methods have been utilized to improve the estimation accuracy and robustness. A pyramid coarse-to-fine strategy is used to deal with large motions more than one pixel. A graduated non-convexity strategy is applied to improve the convergence performance when using a non-convex penalty function. Due to the basic assumptions used in optical flow method, only the flow field with turbulent structures could be resolved.

The velocity contours estimated by the current SME algorithm have been compared with results by an optimized optical flow (OF) method [26]. The OF method is based on traditional smoothness constraint assumptions and advanced optimization techniques to improve the robustness [30]. It is worth mentioning that the constraints imposed on the SME method are only valid for schlieren images, while the constraints in the OF method are more general and can be applied to various forms of images. The accuracy of the OF algorithm has been evaluated using the Middlebury benchmark test database [30]. The estimated average endpoint error (EPE) is 0.319 pixel/frame, which corresponds to a flow speed error at 0.023 m/s with the current experimental setup. As shown in Fig. 3, the SME algorithm shows a comparable velocity range with both the OF and LES results. The OF results can generally resolve the overall velocity in a reasonable range. However, the OF results have shown block structures in the velocity contours, which indicates lower resolution. In contrast, the SME results have shown finer flow structures and also smoother flow field.
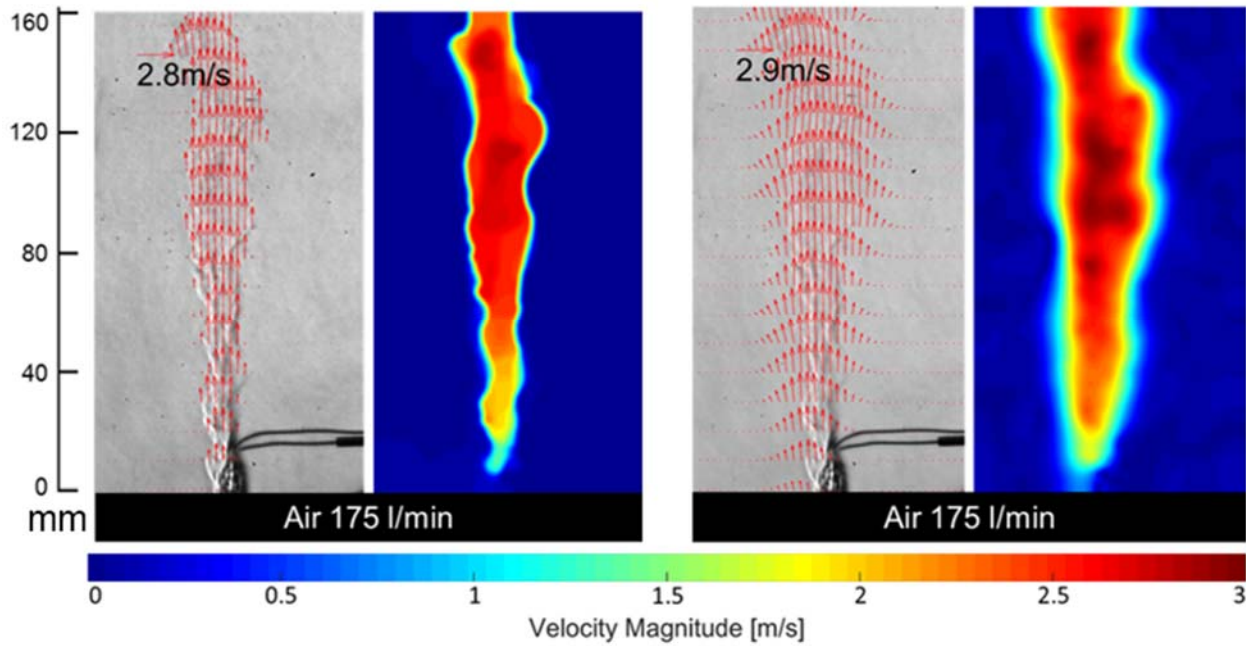

Fig. 3 Comparison of velocity field of OF and SME results [26]

3. Results and discussion

3.1 Cold flow pattern before ignition

The pattern of cold flow before ignition under different conditions has been visualised through schlieren images, as demonstrated in Fig.4. It can be observed that a jet flow is formed from the nozzle exit, which is laminar near the nozzle and transits to turbulent in the downstream region. The height of the laminar pattern is increasing with the increasing of hydrogen percentage. This is mainly due to the fact that under current test conditions, the total volume of the fuel mixture is constant, while the increase in hydrogen percentage will lead to the decreasing of Reynolds number. A turbulent boundary layer is formed near the solid wall due to the impinging effect.
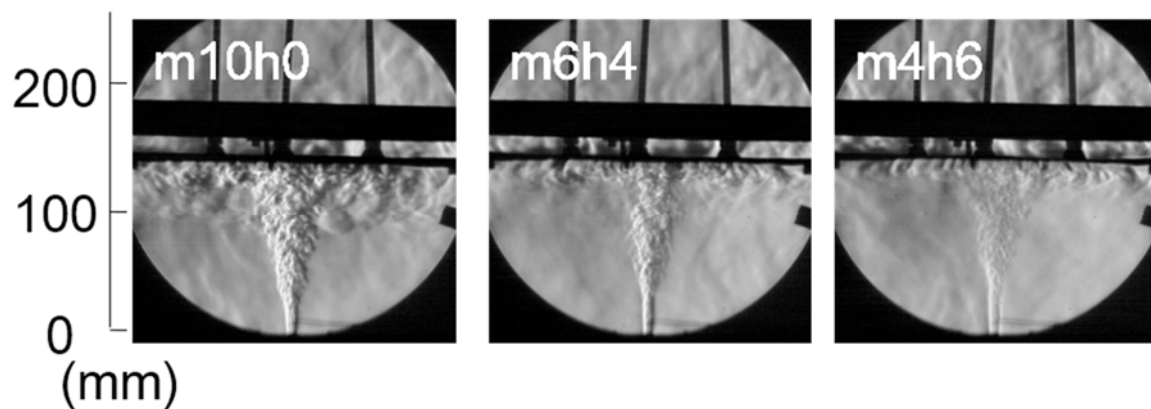

Fig. 4 Cold flow pattern before ignition under different test conditions

3.2 Flame dynamics during ignition process

The time-resolved blue colour enhanced imaging sequences for the tested cases are shown in Fig. 5, while the white line indicates the plate position. By comparing the colour and schlieren images, it is found that the blue flame front is in accordance with the flame front in schlieren images, which demonstrates that the flame structure can be completely revealed using DFCD method. Both blue and yellow-reddish flame can be observed during the ignition process, which indicates the co-existence of both premixed and non-premixed combustion modes during the ignition process. Although the fuel is not premixed with air before it exits the nozzle, a partially premixed mixture will be formed once it mixes with the surrounding air. The existence of premixed flame during the ignition process of diffusion flames has also been recognised in references [17-19]. After the ignition initiation, the flame propagates upwardly from the nozzle exit. The blue flame locates at the flame front, which is mainly propagating in the fuel/air mixing region formed before the ignition started. The yellow reddish

12

diffusion flame is formed following the blue flame front, while the colour mainly comes from the continuous carbon and soot emission from the non-premixed combustion. When the flame reaches the solid disc, it begins to expand from the plate centre outwardly, which forms a blue ring flame. A similar blue disc flame can be observed at 120 ms, 80 ms, and 60 ms for m10h0, m6h4 and m4h6 respectively. It means that the flame propagation speed is increasing with the increase of hydrogen percentage even though the Reynolds number is decreasing. The reason lies in the fact that hydrogen has a much higher burning velocity than methane. The yellow-reddish diffusion flame occurs following the blue flame front and a stable impinging diffusion flame will establish at the end of the ignition process in all the cases. It can be observed that part of the flame has extended over the plate position, for two main reasons. First of all, the photograph of the flame is taken at a tilted angle to show more flame structures. Thus the white line in Fig. 5 is only an approximate indication of the centre line shown in the image. The other reason is that the plate has a diameter of 300 mm, and some fuel/air mixtures may go beyond the plate, which causes the flame to propagate over the plate.
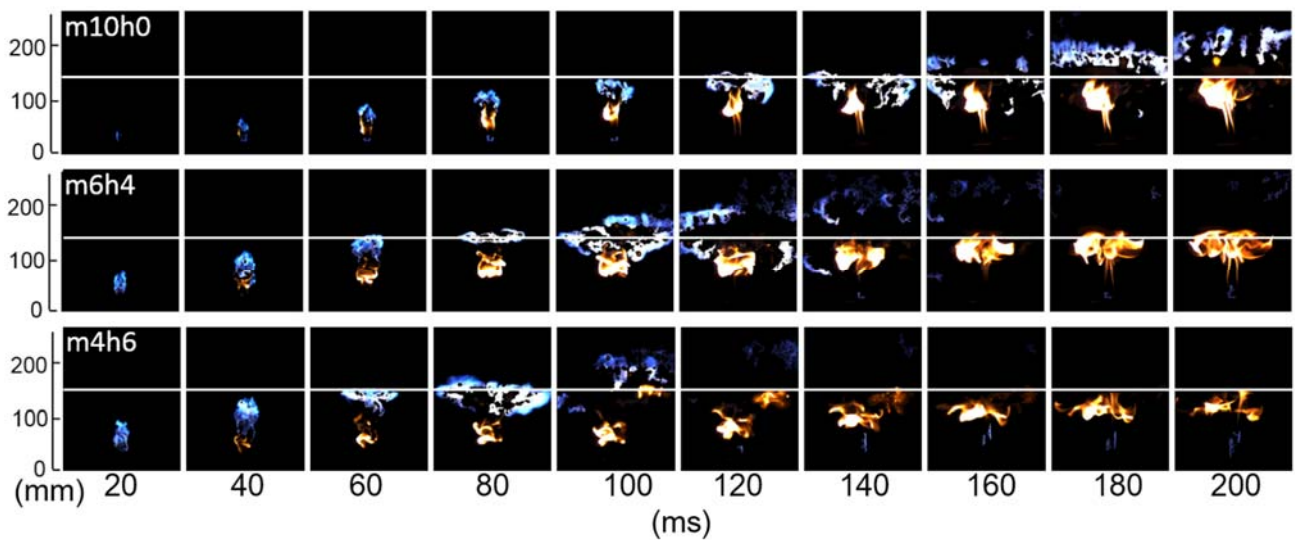

Fig.5 Colour image sequences with different hydrogen percentage
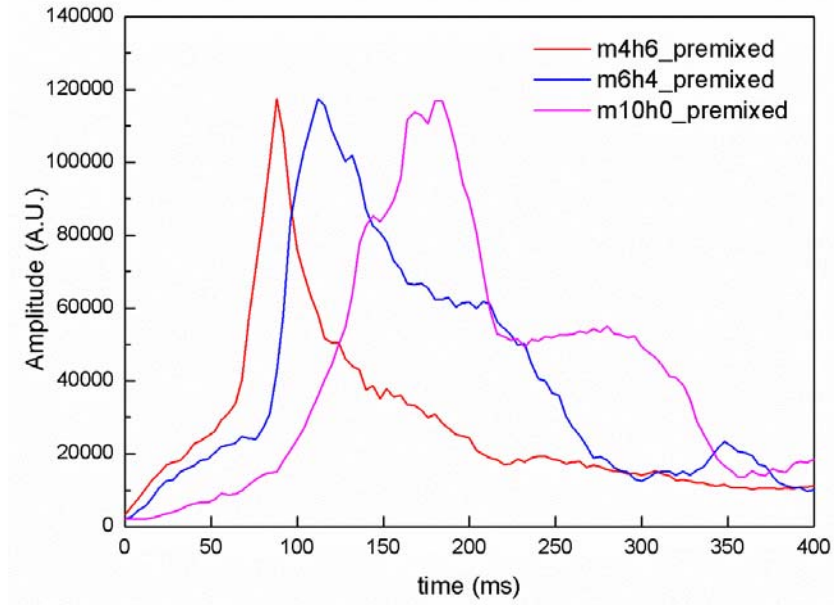(with blue colour enhanced by 15 times)

Based on the DFCD results, the blue colour corresponding to premixed flame can be discriminated and used for further analysis. The integration of blue colour intensity is able to model well the CH* chemiluminescence emission [18]. The variance of the blue flame intensity at different time instants has been presented in Fig.6(a). It can be seen that there is a peak value for premixed

13

flame intensity in each case, which is similar for the four cases. With the increasing of hydrogen percentage, the time reaching the peak value is decreasing, which is 184 ms, 112 ms, and 88 ms for m10h0, m4h6 and m6h4 respectively. The overall CH* chemiluminescence emission during the ignition process can be obtained from an intensity integration with time, which decreases when the hydrogen percentage is increased. It can be seen from Fig.5 that the peak value occurs when the flame propagates radially to the edge of the plate, where a blue disc flame is formed by consuming the accumulated fuel/air mixtures.
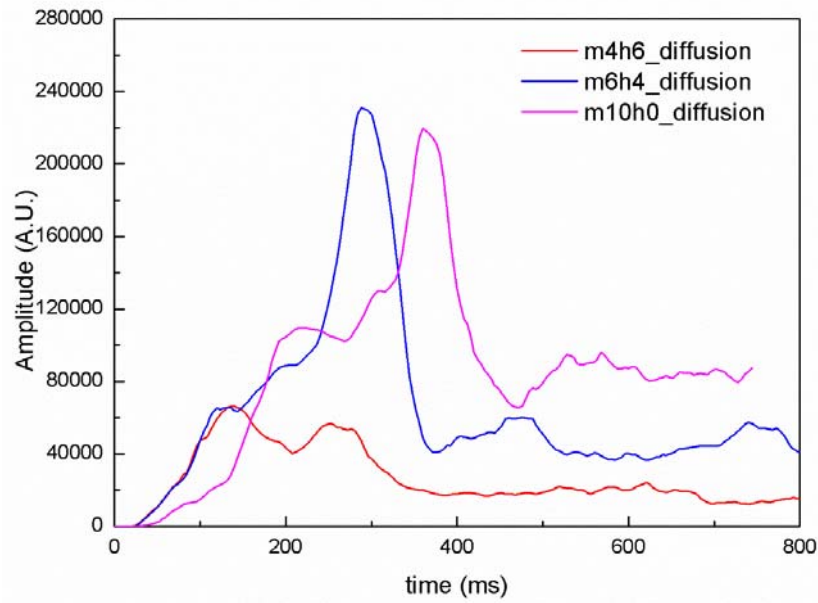
By excluding the blue flame region, the diffusion flame intensity variation with time has been presented in Fig. 6(b). For all the cases, the diffusion flame intensity increases with time first and then decreases gradually after the peak value. The peak value occurs at 360 ms, 288 ms and136 ms for m10h0, m4h6 and m6h4 respectively. It is noticed that the diffusion flame peak value appears later than the premixed flame peak value in each case, which is in accordance with the phenomena that the diffusion flame develops following premixed flame front. The two cases m10h0 and m6h4 have shown comparable intensities during the ignition process, while a dramatic decrease occurs for m4h6. This may be due to the saturation effect when the flame intensity is too high. Very bright flame regions can be observed for the cases of m10h0 and m6h4, which will lead to underestimation of the diffusion flame intensity. From the images, it can be seen that m10h0 has more saturation regions than m6h4. Thus the actual diffusion flame intensity of m10h0 should be higher than m6h4. On the whole the intensity of the yellow reddish flame is decreasing with the increase of hydrogen percentage. This is consistent with the observation that when a stable diffusion flame is formed after 500 ms, without the saturation effect, the diffusion flame intensity shows a gradually decreasing trend with increasing hydrogen percentage.

The differences among the three cases are mainly attributed to two factors. First, with increasing percentage of hydrogen, the diffusivity of the fuel mixture is increased, which makes fuel-air mixing faster. As a result, the premixed flame is increasingly dominant while the diffusion flame becomes relatively weak, for the same fuel supply rate. Second, increasing hydrogen percentage reduces the

14

carbon content and thus the intensity of the yellow-reddish flame. The trends shown in both Figs. 6(a) and (b) are in line with the above analysis.

(a)

(b)

Fig.6 (a) Premixed and (b) diffusion flame intensity variation during the ignition process

3.3 Flow field visualization and velocity estimation based on schlieren images

A previous study has measured the laminar burning velocity of methane/hydrogen mixtures with different compositions and equivalence ratios [3]. As shown in Fig.7, it can be seen that, the laminar burning velocity increases with increasing hydrogen percentage. However, the effect of hydrogen

enrichment is highly nonlinear. The laminar burning velocity increases slightly when the hydrogen percentage is no more than 40%. A considerable increase can be observed at 60% hydrogen percentage. Remarkably, the increase in the laminar burning velocity becomes dramatic when the hydrogen percentage reaches 80% and finally, 100%.
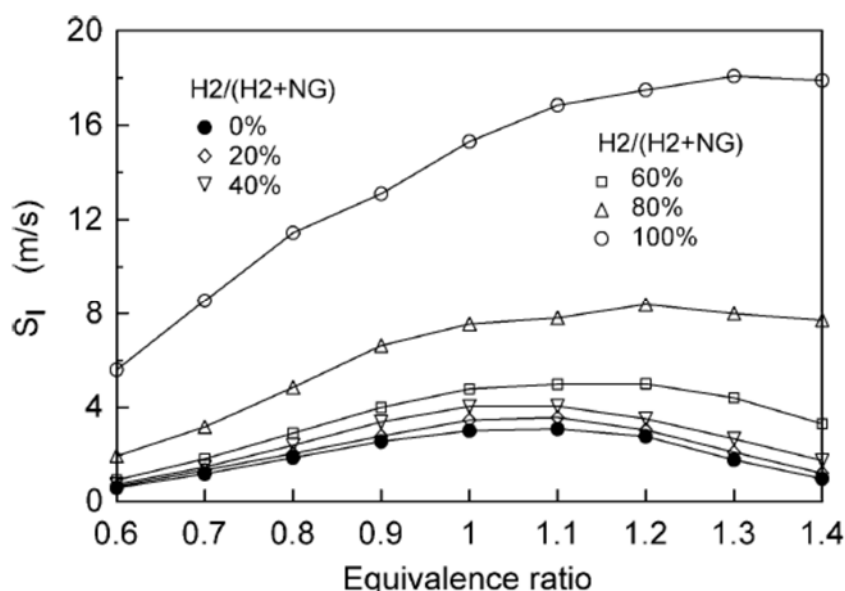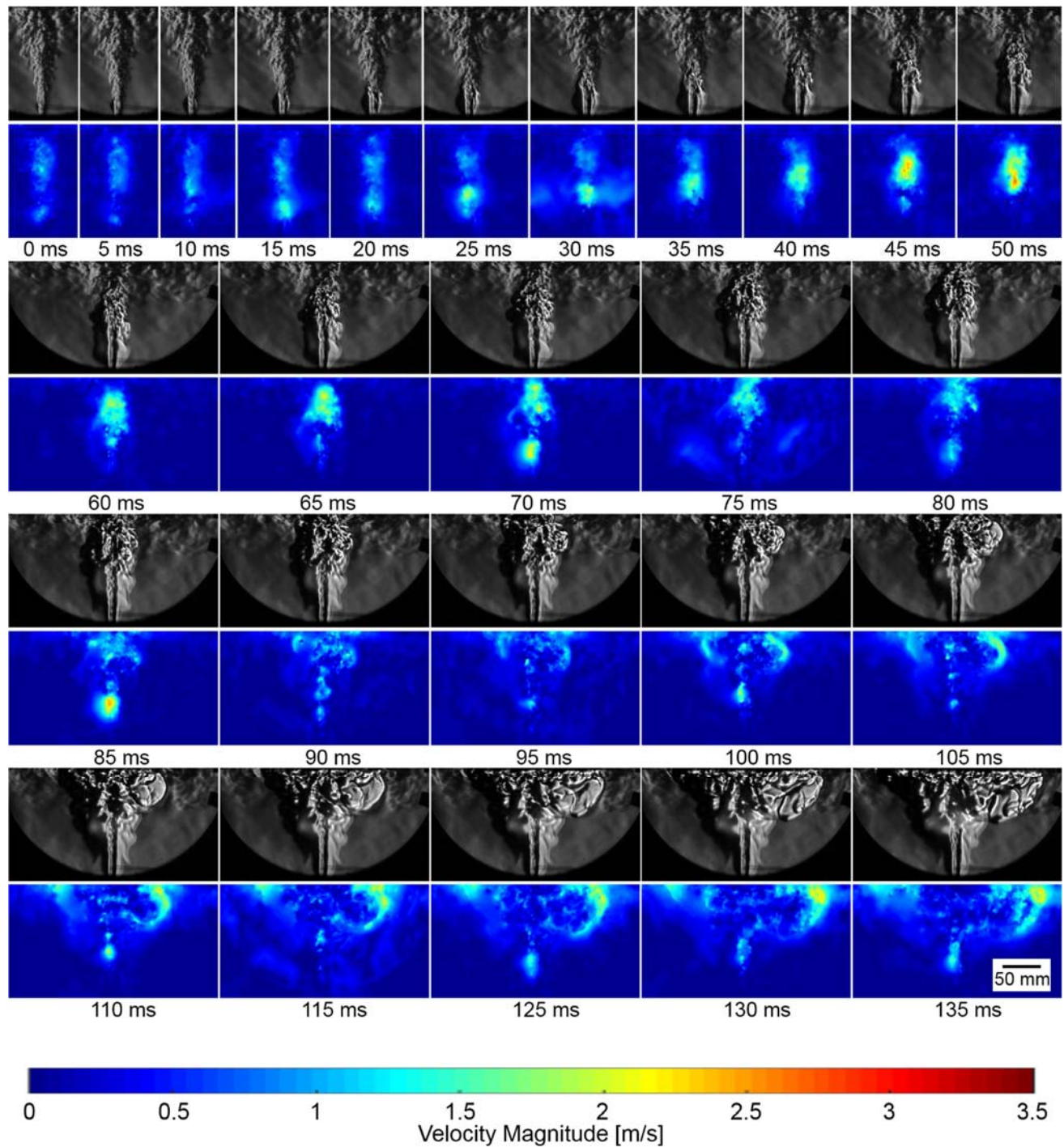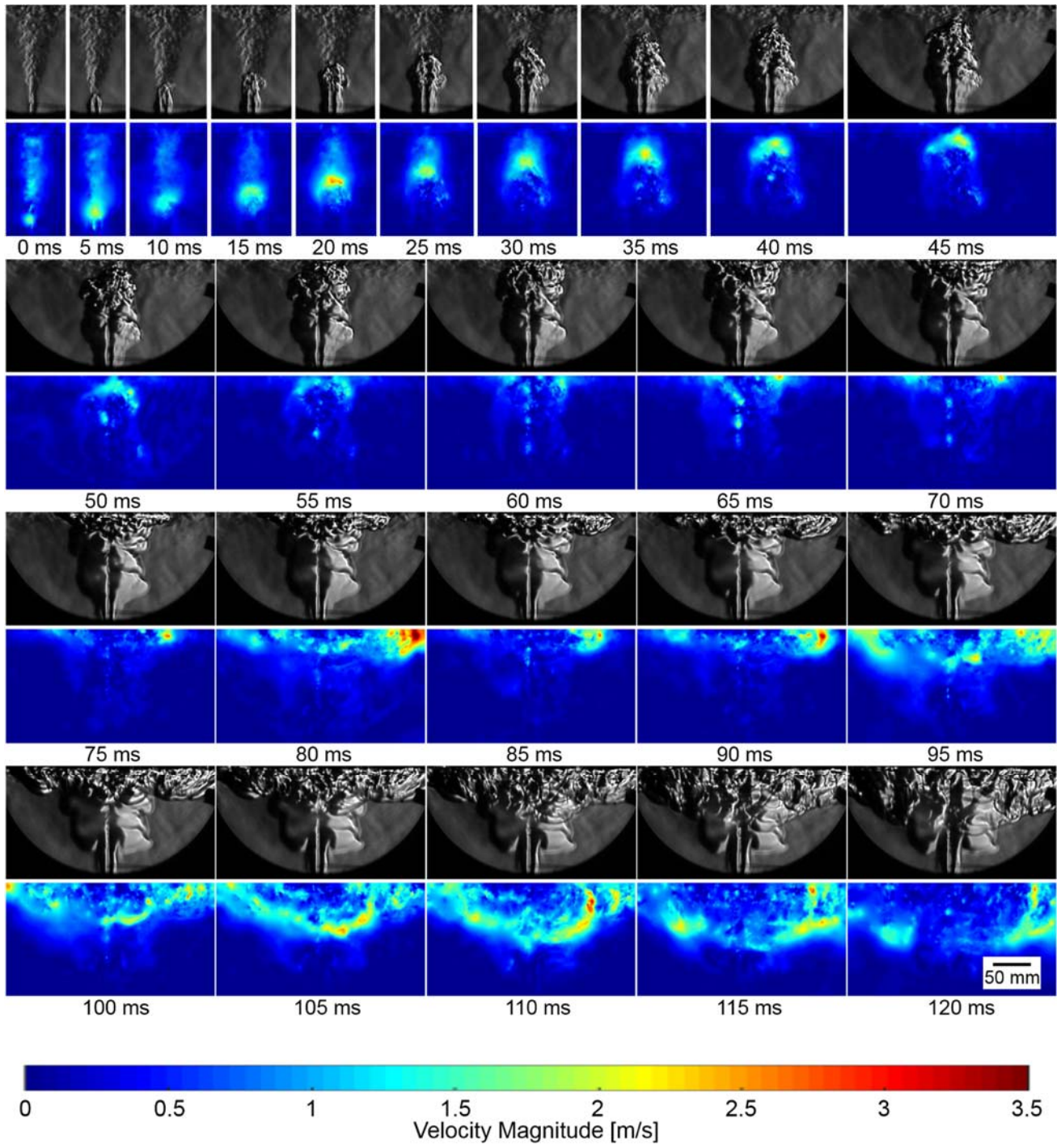

Fig. 7 Unstretched flame speed versus equivalence ratio at various hydrogen fractions [3]

In the current study, the flow field during the ignition process has been visualized by high speed schlieren images, while the flow field velocity was estimated using the schlieren motion estimation (SME) method. The schlieren images and velocity contours of different cases have been presented in Fig.8. It can be seen that the flame is propagating upward in the jet region and begins to propagate radially after reaching the impinging plate. With the increasing of hydrogen percentage, the flow field velocity is increasing. During the upward process, the maximum velocity occurs at the flame front. The time from ignition to the end of the upward process is 75 ms, 55 ms and 45 ms for m10h0, m6h4, and m4h6 respectively. After the impingement, the outward propagation begins. The velocity is decreasing to lower values and then increasing when the flame approaches the mixing layer near the edge of the plate. After that a diffusion flame is formed and the velocity decreases to lower values. The maximum velocity during the ignition process occurs during the outward process. When the fuel impinges on the plate, it will spread along the plate area and form a thin turbulent boundary layer.
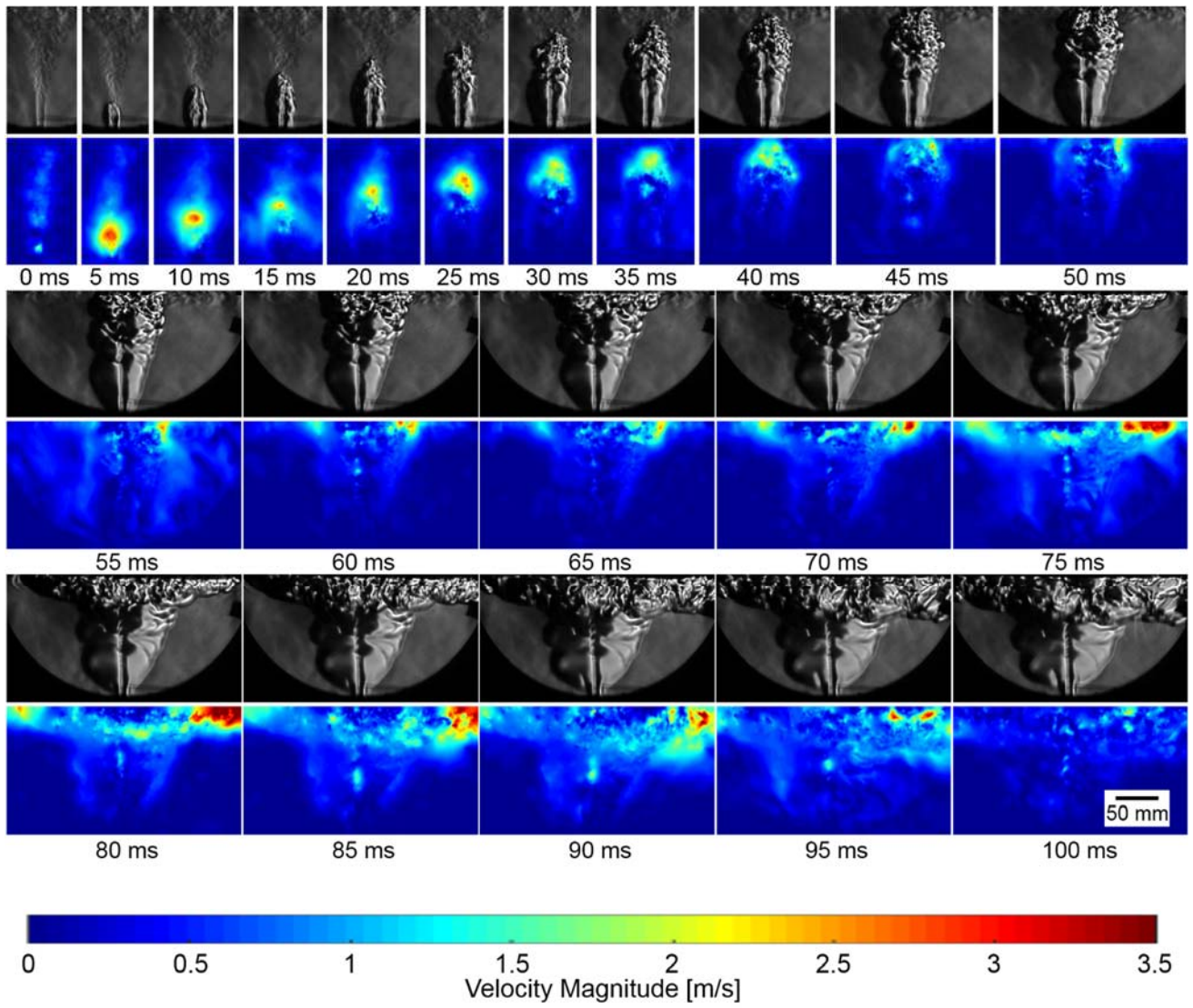
Comparing with the jet region, the boundary layer will have a much larger area in contact with air, which will lead to better fuel/air mixing with strong turbulence intensity. Also the heat release from previously formed flame may increase the temperature of the fuel/air mixture. Under dual effects, a faster flame propagation can be observed in this region. For the pure methane case, the maximum velocity is about 2.5 m/s, while it is 2.8m/s for the case of m6h4. For the cases m4h6, the maximum value is over 3.5 m/s.

(a) m10h0

(b) m6h4

18

(c) m4h6

Fig. 8 Schlieren images and velocity contours of different mixtures

(a) m10h0 (b) m6h4 (c) m4h6

Based on the velocity contours, the relative velocity between the flame and flow can be resolved following the procedures described here. Firstly, three neighbouring schlieren images at time steps $n-1$, n and $n+1$ are selected. Thus two velocity contours can be obtained with two pairs of neighbouring images, i.e. $n-1$ and n, n and $n+1$. Secondly, the flame front at the time step n is identified using image processing techniques shown in Fig.9. The flame structure is identified based on the pixel intensity and the binary image is generated. The boundary of the whole flame structure is extracted, while the flame front is selected manually based on the observation from schlierern images. The flame velocity

19

is obtained by reading the velocity vectors on the flame front line. The flow velocity is obtained using the identical flame front but on the velocity contour at a previous time step. Finally, the relative velocity is calculated using the flame velocity to subtract the flow velocity at the same position. The results at different time instances with 10 ms time internals are presented in Fig.10. For all the three cases, the flame fronts are seen to move upward first and then propagate radially. For the same time intervals, the flame fronts are distributed more sparsely with the increase of hydrogen percentage, which is consistent with the increased flame propagation speed. For each case, the relative velocity is high during the upward movement but decreases to lower values during the impinging process on the wall before increasing again during the outward process. This is roughly in accordance with the absolute velocity change shown in Fig. 8. The relative velocity during the initial upward process has shown different behaviours, with m10h0 the highest, m4h6 the lowest and m6h4 in the middle. This may be due to the variance in the flame front shape. It can be seen that the flame front is narrower for m10h0, flatter for m4h6 and much flatter for m6h4. For a narrower flame front, its velocity will be higher according to the mass conservation equation. During the outward propagating stage, the relative velocity increases with higher hydrogen percentage. For cases m6h4 and m4h6, the maximum relative velocity is about 1.4 m/s, which occurs around the plate edge.
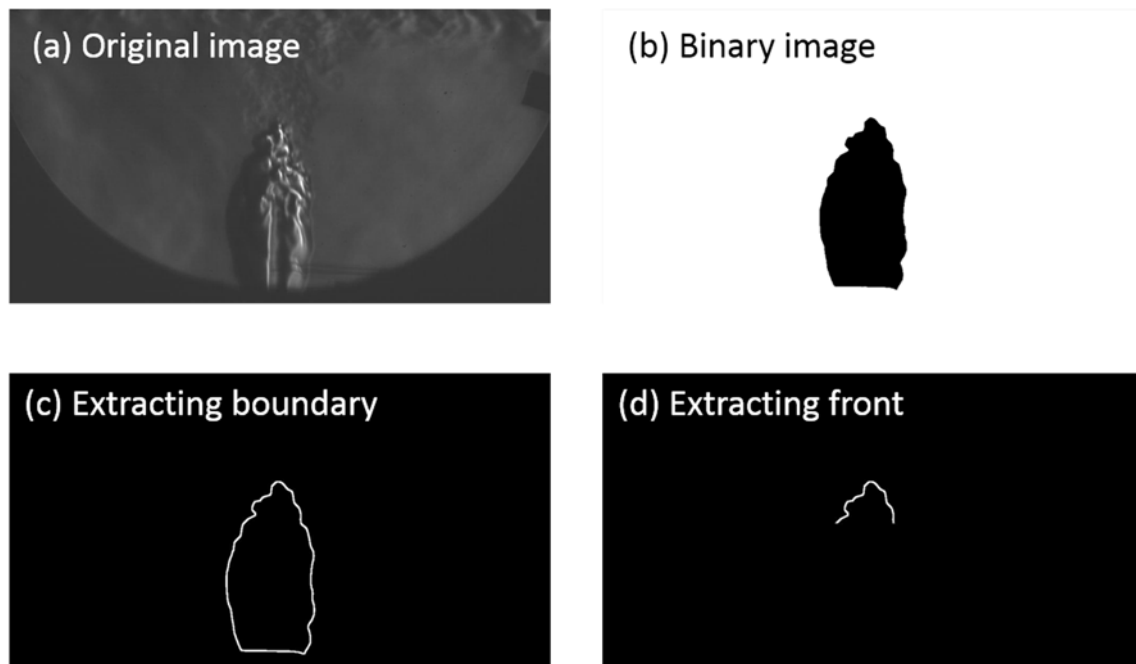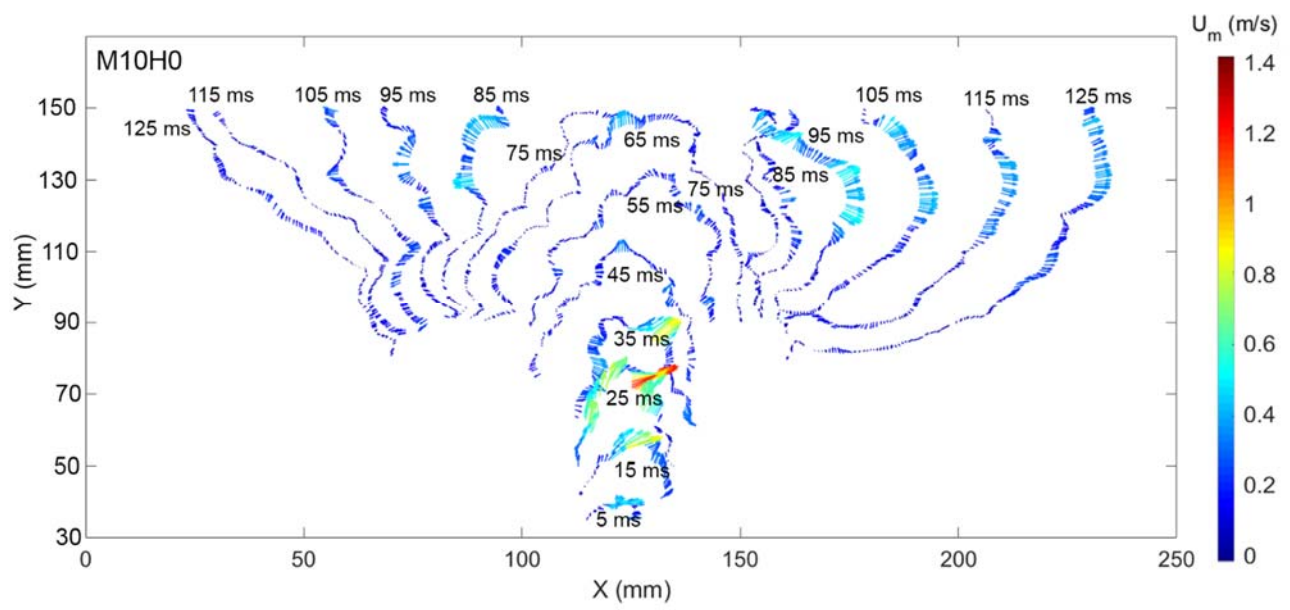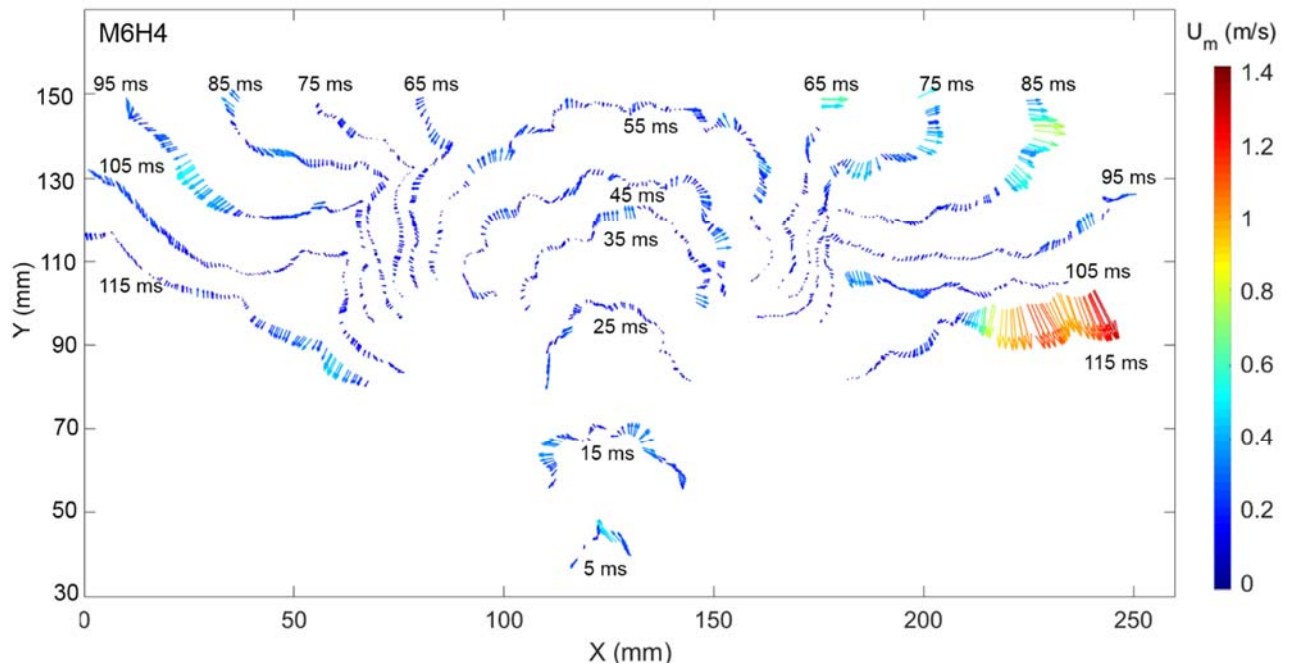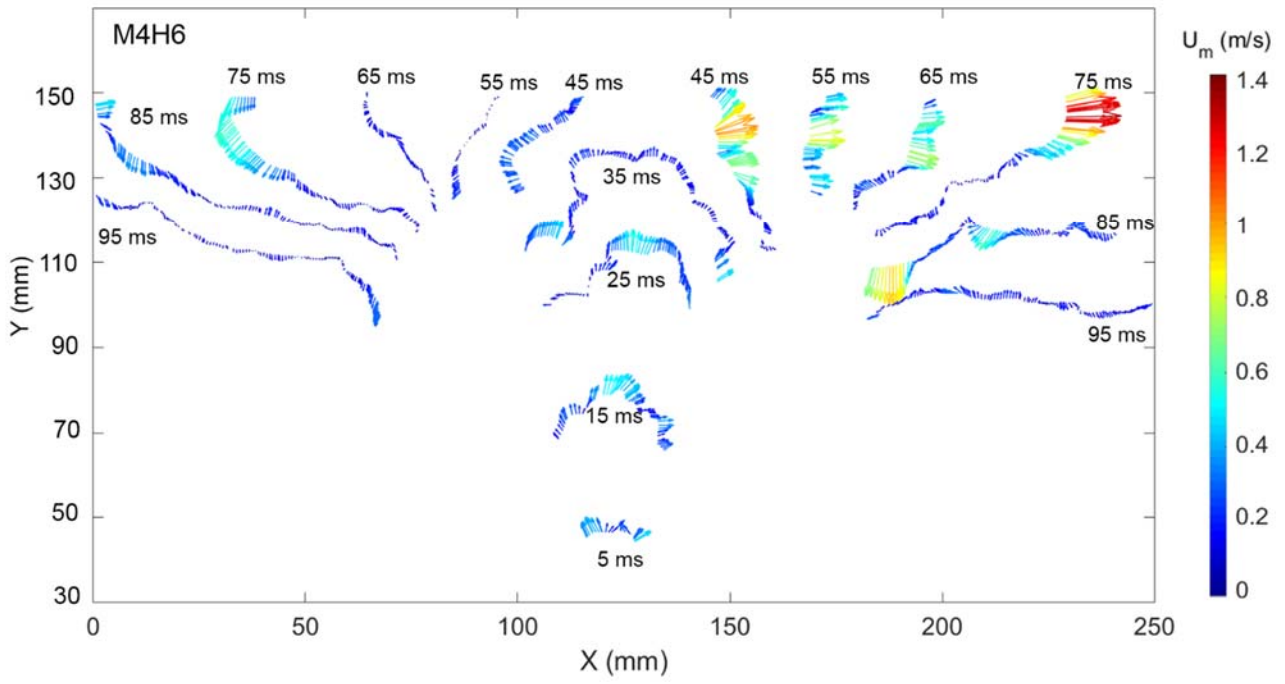

Fig. 9 Image processing procedures for extracting the flame front

(a)

(b)

(c)

Fig. 10 Relative velocity between flame and flow at different time instants of

(a) m10h0 (b) m6h4 and (c) m4h6

4. Conclusion

In this study, the ignition characteristics of hydrogen enriched methane diffusion impinging flames with different fuel compositions have been investigated experimentally. In the experimental setup, two visualisation techniques are employed: high speed colour and schlieren imaging. Combining these with advanced image processing techniques, the flame front, flame colour and flow field structure during the fast transient ignition process have been shown clearly. In the meantime, the quantitative velocimetry was conducted on schlieren images specifically. A colour discrimination algorithm is applied to digitally enhance the weak blue chemiluminescence, which helps to show the complete flame structure during the ignition process. Premixed blue flame has been observed at the flame front, which is due to the air/fuel mixing effect at the jet shear layer and the boundary layer near the solid wall. The appearance of reddish soot flame is at a later stage than chemiluminescence. Both the CH* chemiluminescence and soot flame intensity decrease with increasing hydrogen percentage, due to the increased diffusivity and decreased carbon content in the fuels. The quantitative information about

22

the velocity of the flow field has been obtained using a novel schlieren motion estimation method. The relative velocity at the flame front has also been resolved and analysed. The velocity contour shows that the flame propagation velocity increases with increasing hydrogen volume percentage, mainly because of the higher burning velocity of hydrogen. The maximum velocity appears when the flame propagates to the plate edge, where the turbulent boundary layer leads to better fuel/air mixing. The relative velocity has shown more complex variations. Strong variations of the velocity amplitude and direction can be observed on each flame front and also at different time instants. At the initial upward stage, it is smaller with the increase of the hydrogen percentage, which may be attributed to the enlarged flame front area. During the radial propagation period, the relative velocity shows an increasing trend with the increase of hydrogen percentage. These quantitative measurements provide rich information about the fast transient ignition process, which shed a light on the complex phenomena of ignition of methane/hydrogen mixtures under impinging conditions and potentially serve as a validation database for future simulation results. The proposed techniques are effective, low-cost and convenient to use, which show a great potential for hydrogen enriched combustor stability studies.

Acknowledgements

References

[1] S.R. Bell, M. Gupta, Extension of the lean operating limit for natural gas fuelling of a spark ignited engine using hydrogen blending, Combust. Sci. Technol. 123 (1997) 23-48.

[2] R. Stephen, An Introduction to Combustion: Concepts and Applications, McGraw-Hill, Boston, U.S., 2000.

[3] Z.H. Huang, Y. Zhang, K. Zeng, B. Liu, Q. Wang, D.M. Jiang, Measurements of laminar burning velocities for natural gas-hydrogen-air mixtures, Combust. Flame 146 (2006) 2385-2390.

[4] E. Hu, Z.H. Huang, J.J. He, C. Jin, J.J. Zheng, Experimental and numerical study on laminar burning characteristics of premixed methane/hydrogen/air flames, Int. J. Hydrogen Energ. 34 (2009) 4876-4888.

[5] E. Mastorakos, Ignition of turbulent non-premixed flames, Prog. Energy Combust. Sci. 35 (2009) 57-97.

[6] T.X. Phuoc, C.M. White, D.H. McNeill, Laser spark ignition of a jet diffusion flame, Opt. Laser. Eng. 38 (2002) 217-232.

[7] E.S. Richardson, E. Mastorakos, Numerical investigation of forced ignition in laminar counterflow non-premixed methane-air flames, Combust. Sci. Technol. 179 (2007) 21-37.

[8] T. Jin, K.H. Luo, X. Wang, K. Luo and J. Fan, Dynamics of triple-flames in ignition of turbulent dual fuel mixture: a direct numerical simulation study, Proc. Combust. Inst. 37 (2019) 4625-4633.

[9] P. Rajpara, R. Shah, J. Banerjee, Effect of hydrogen addition on combustion and emission characteristics of methane fuelled upward swirl can combustor, Int. J. Hydrogen Energy, 43 (2018) 17505-17519.

[10] T. Hussain , M. Talibi , R. Balachandran, Investigating the effect of local addition of hydrogen to acoustically excited ethylene and methane flames, Int. J. Hydrogen Energy 44 (21) (2019) 11168–11184 .

[11] G. Oztarlik, L. Selle, T. Poinsot, T. Schuller, Suppression of instabilities of swirled premixed flames with minimal secondary hydrogen injection, Combust. Flame 214 (2020) 266-276.

[12] X. Jiang, H. Zhao, K.H. Luo, Direct numerical simulation of a non-premixed impinging jet flame, J. Heat Trans. 129 (2007) 951-957.

[13] Y. Zhang, K.N.C. Bray, Characterization of impinging jet flames, Combust. Flame 116 (1999) 671-674.

[14] D. Durox, T. Schuller, S. Gandel, Self-induced instability of a premixed jet flame impinging on a plate, Proc. Combust. Inst. 29 (2002) 69-75.

[15] X. Jiang, K.H. Luo, L. de Goey, R. Bastiaans, J.A. van Oijen, Swirling and impinging effects in an annular nonpremixed jet flame. Flow Turbul. Combust. 86(1) (2011) 63-88.

[16] K.R. Dinesh, X. Jiang, J.A. van Oijen, Numerical simulation of hydrogen impinging jet flame using flamelet generated manifold reduction. Int. J. Hydrogen Energ. 37(5) (2012) 4502-15.

[17] Q. Wang, C.Y. Zhao, Y. Zhang, Time-resolved 3D investigation of the ignition process of a methane diffusion impinging flame, Exp. Therm. Fluid Sci. 62 (2015) 78-84.

[18] Q. Wang, H.W. Huang, Y. Zhang, C.Y. Zhao, Impinging flame ignition and propagation visualization using schlieren and colour-enhanced stereo imaging techniques, Fuel 108 (2013) 177-183.

[19] Y. Chen, T. Yao, Q. Wang, K.H. Luo, Large eddy simulation of impinging flames: Unsteady ignition and flame propagation, Fuel 255 (2019) 115734.

[20] A.G. Gaydon, The Spectroscopy of Flames, Chapman and Hall, Harlow, U.K., 1974.

[21] H.W. Huang, Y. Zhang, Flame colour characterization in the visible and infrared spectrum using a digital camera and image processing, Meas. Sci. Technol. 19 (2008) 085406.

[22] G.S. Settles, Schlieren and shadowgraph techniques: visualizing phenomena in transparent media, Springer, Germany, 2001.

[23] S. Fu, Y. Wu, Detection of velocity distribution of a flow field using sequences of schlieren images, Opt. Eng. 40 (2001) 1661-1666.

[24] T. Corpetti, É. Mémin, P. Pérez, Dense estimation of fluid flows, IEEE T Pattern Anal. 24 (2002) 365-380.

[25] E. Arnaud, E. Mémin, R. Sosa, G. Artana, A fluid motion estimator for schlieren image velocimetry, 9th ECCV (2006) 198-210.

[26] Q. Wang, Y. Wu, H.T. Cheng, X.H. Mei, C.Y. Zhao, A schlieren motion estimation method for seedless velocimetry measurement, Exp. Therm. Fluid Sci. 109 (2019) 109880.

[27] D. Suter, Motion estimation and vector splines, IEEE CVPR 94(1994) 939-942.

[28] A. Buades, B. Coll, J.-M. Morel, A non-local algorithm for image denoising, IEEE CVPR (2005) 60-65.

[29] G. Gilboa, S. Osher, Nonlocal operators with applications to image processing, Multiscale Model. Sim. 7 (2008) 1005-1028.

[30] D. Sun, S. Roth, M.J. Black. Secrets of optical flow estimation and their principles. IEEE CVPR, 2010.